Perturbative QCD calculations of weak-boson production in association with jets at hadron colliders

V. Barger and T. Han
Physics Department, University of Wisconsin, Madison, Wisconsin 53706

J. Ohnemus
Physics Department, Florida State University, Tallahassee, Florida 32306

D. Zeppenfeld
Physics Department, University of Wisconsin, Madison, Wisconsin 53706

(Received 17 May 1989)

We present perturbative QCD calculations of $W,Z+n$-jet production ($n \leq 3$) in $p\bar{p}$ collisions at $\sqrt{s}=0.63$ and 1.8 TeV and also extrapolate the production cross sections to supercollider energies. The dependence of the cross sections on experimental cuts and the theoretical ambiguities are discussed in detail. It is shown that W/Z ratios of transverse-momentum distributions are quite insensitive to these uncertainties and can be predicted rather accurately. Neutrino counting and a top-quark search at large p_T are addressed as applications. Our results are based on complete tree-level calculations of $W,Z+(n+2)$-parton amplitudes.

I. INTRODUCTION

The study of weak-boson production at hadron colliders[1-9] has been of great interest in recent years for a number of reasons. First, detailed studies on the properties of weak bosons provide precise tests of the standard $SU(2)_L \otimes U(1)_Y$ electroweak gauge theory. Second, the strong-interaction part of the standard model (SM) can be further scrutinized in the production of weak bosons in association with hard QCD jets.[4-11] Third, potential new physics could manifest itself with W,Z bosons as the decay products of new particles. Examples of new physics include heavy quarks,[12] heavy Higgs bosons,[13] heavy supersymmetric particles,[14] an extra Z boson, and exotic scalars and fermions in superstring-inspired models.[15] In neutrino counting[16] and a top-quark search,[17] the direct W,Z-boson production cross sections must be quantitatively known. Therefore, a complete understanding of weak-boson production within the SM is essential to identify any new physics in collider experiments.

Since the discovery of the W and Z bosons at the CERN $p\bar{p}$ collider (S$p\bar{p}$S) in 1983 (Ref. 1), there have been further measurements of W,Z production[2] at c.m. energy $\sqrt{s}=0.63$ TeV. An integrated luminosity of order 5 pb^{-1} may be taken by both UA1 and UA2 by the end of the current run. Recently, the Collider Detector at Fermilab (CDF) Collaboration working at the Tevatron has reported on W-boson production[3] at $\sqrt{s}=1.8$ TeV. By the end of the current CDF run, an integrated luminosity of about 5 pb^{-1} is expected and of order 100 pb^{-1} should be accumulated in future runs. The inclusive cross sections of W- (Z-) boson production are about 6 (1.8) nb at the CERN $p\bar{p}$ collider and 21 (6.3) nb at the Tevatron. Thus large samples of W,Z bosons will be obtained at the S$p\bar{p}$S and the Tevatron, and in the future enormous numbers of weak bosons could be produced at the CERN Large Hadron Collider (LHC) and the Superconducting Super Collider (SSC).

On the theoretical side, several authors have evaluated the production of $W,Z+1,2$ jets, both at the tree level[5-7] and including radiative corrections,[4] and found good agreement with data from the CERN $p\bar{p}$ collider. In a recent Letter we presented expectations[8] for the production of $W,Z+n$ jets ($n=1,2,3$) at the Tevatron and Berends *et al.* have since presented similar results[9] including the S$p\bar{p}$S energy.

The purpose of this paper is to provide additional information on the production of W,Z bosons in association with n QCD jets ($n \leq 3$) at hadron colliders. We discuss in more detail the anticipated experimental problems of comparing theory and experiment and we elaborate on the theoretical ambiguities as well as the definite predictions of our calculations. The remainder of this paper is organized as follows. In Sec. II we discuss the calculational techniques used in our work and comment on our checks with other analyses. In Sec. III we present our major results. We evaluate the total cross sections versus c.m. energy at hadron colliders and present relevant dynamical distributions at $\sqrt{s}=0.63$ and 1.8 TeV. We present Z-to-W production ratios which are needed for neutrino counting and for top-quark searches. These ratios are essentially independent of the choice of the scale Q^2 in the strong coupling constant α_s. In Sec. IV we discuss the uncertainties of the calculations resulting from the kinematical cuts, from different choices of quark and gluon distributions, and from the freedom of choosing different scales Q^2 in α_s. The QCD predictions for $W,Z+3$-jet events can differ by as much as a factor of 3 with various choices of the Q^2 scale. Finally, in Sec. V we summarize our results.

II. CALCULATIONAL FRAMEWORK

The calculation of weak-boson production in association with jets becomes increasingly difficult as the number of jets increases. The traditional trace method of evaluating the squared matrix element of the process is not very practical for the case of two or more jets; instead it is easier to derive analytic expressions for the amplitudes which are first evaluated numerically and then squared to give the differential cross sections. Several amplitude-level techniques have been used for calculating W,Z production at large transverse momentum (p_T) in the framework of perturbative QCD (Refs. 5–9). General tree-level amplitudes of one electroweak vector boson V ($V=W^{\pm}$, Z, and γ) plus up to five colored partons were first presented by Hagiwara and Zeppenfeld,[10] using the amplitude technique developed in Ref. 18.

The analytic expressions of Ref. 10 include the decay of the W or Z into a lepton pair and complete expressions of all the cross-section formulas are given including the handling of color factors. Our calculations are based on these results and hence include the W and Z decays with full spin correlations of the decay products. We allow the weak bosons to be off shell in general. We also include virtual-photon contributions along with the Z in the e^+e^- channel.

For the numerical work of the present paper a computer program of all the amplitudes of Ref. 10 was developed,[19] which allows the evaluation of the differential cross sections for all the underlying parton-level subprocesses leading to $W,Z+n$ jets ($n\leq 3$) in $\bar{p}p$ collisions. Since the amplitudes have to be evaluated numerically for fixed polarizations of the external particles and for fixed quark flavors (u,d,c,s,b), the final task is to sum over the possible polarization states and all possible contributing channels (205 for $Z+3$ jets and 158 for W^++3 jets). We include the contributions of the five light-quark flavors in the massless quark approximation. For W production we neglect Cabibbo-Kobayashi-Maskawa mixing. This introduces a very small error through the different structure functions for d, u, s, and c quarks. (We neglect b quarks as constituents of the proton.) The effect is small already for $W+0$-jet production (less than $\sin^2\theta_C\approx 4\%$) and is further reduced for events with jets in which initial-state gluons play an important role.

The sum over polarization states of quarks and gluons was performed both by direct and by Monte Carlo summation. In the latter method one particular polarization state is randomly chosen as representative for each event. Since for the worst case of $Z\rightarrow e\bar{e}$ with two fermion pairs and three gluons in the initial and final states there are 32 different polarization combinations, up to a factor of 32 can be gained in speed by random polarization summation. In practice, however, the efficiency of the Monte Carlo program will suffer somewhat, requiring a larger number of events to be generated in order to produce distributions of the same statistical quality as for explicit summation of polarization states. The bottom line is that we find about an order-of-magnitude improvement in speed due to Monte Carlo summation.

In Table I we summarize the CPU time needed on a VAX 8700 for the calculation of $W,Z+3$-jet production. The numbers are for random polarization summation. In the Z case, the number of calls for the cross sections of the basic subprocesses, either involving two quarks and three gluons or four quarks and one gluon, are considerably smaller than in the W case, because our program simultaneously calculates the two subprocesses related by charge conjugation. For W production, on the other hand, we only use CP invariance, which in $\bar{p}p$ collisions implies equality of the W^+ and W^- rates and hence gives a trivial overall factor of 2. By comparing the time needed per accepted event (the last column of Table I) and the time needed for the subprocess calls, one finds that a considerable fraction of the CPU time is spent in setting up phase space, organizing the output, etc.; the basic subprocess calculations have to be considered as extremely fast.

We have checked our numerical calculations against other sources. It is fairly easy to confirm the correctness for the $V+1$-jet channel, since the calculation is simple in this case. In order to check our $V+2$-jet programs we have compared our calculations with those of Kleiss and Stirling[5] at $\sqrt{s}=0.63$ TeV and with evaluations of the analytic formulas of Ellis and Gonsalves.[7]

By now two additional independent calculations of cross sections for one electroweak boson and five partons exist: Berends, Giele, and Kuijf[11] have used a different helicity amplitude technique[20] and recursive methods[21] to evaluate the underlying amplitudes numerically, while Falck, Graudenz, and Kramer[22] recently presented numerical results on $e^+e^-\rightarrow 5$ jets, which were based on a REDUCE calculation of the partonic differential cross sections. A numerical comparison of subprocess differential cross sections at individual phase-space points for all the $W+n$-jet processes ($n\leq 3$) and for $e^+e^-\rightarrow 5$ jets (including s-channel photon and Z exchange) yielded complete numerical agreement between our code and the one used by the authors of Refs. 9 and 11. Furthermore, by appropriate crossings, we have reproduced the recent calculation for $e^+e^-\rightarrow 5$ jets in Ref. 22.

III. QUANTITATIVE RESULTS

Using the procedure described in the previous section, we have calculated $V+n$-jet ($n\leq 3$) production in had-

TABLE I. CPU times (in milliseconds) necessary on a VAX 8700 to calculate $p\bar{p}\rightarrow W^-(\rightarrow e^-\bar{\nu})+3$-jet, and $p\bar{p}\rightarrow Z(\rightarrow e^+e^-)+3$-jet events. The "No. calls" column gives the number of basic subprocess calculations needed to evaluate the cross section at one phase-space point.

	Subprocess	No. calls	Time per call (msec)	Time per event (msec)
$W+3$ jets	$qqggg$	7	2.7	80
	$qqqqg$	20	1.8	
$Z+3$ jets	$qqggg$	4	2.7	50
	$qqqqg$	5	2.8	

ron collisions. The SM parameters we have used are $\alpha(M_W)=\frac{1}{128}$, $\sin^2\theta_W=0.23$, $M_Z=91.9$ GeV, and $m_t > M_W = M_Z\cos\theta_W = 80.6$ GeV.

In order to approximately simulate the detector environment, we impose some typical acceptance and resolution requirements, as summarized in Table II. We first take the p_T and η cuts on the electron(s) as given in Table II, where p_T is the transverse momentum and $\eta=\ln(\cot\theta/2)$ is the pseudorapidity of the electron. Electron energy mismeasurements are taken into account by generating a Gaussian smearing of electron energies and momenta with standard deviation $\sigma=(0.15\ \text{GeV}^{1/2})\sqrt{E}$. For W events, we also require a large missing transverse momentum ($\not{p}_T$) due to the escaping neutrino, $\not{p}_T > 15$ GeV. For W,Z identification, we impose $M_T(e,\not{p}_T)$ or $M_{ee} > 50$ GeV, where $M_T(e,\not{p}_T)$ is the W transverse mass,

$$M_T(e,\not{p}_T)=\{[|\mathbf{p}_T(e)|+|\not{\mathbf{p}}_T|]^2-[\mathbf{p}_T(e)+\not{\mathbf{p}}_T]^2\}^{1/2}\ , \qquad (1)$$

and M_{ee} is the invariant mass of the electron-positron pair.

On our parton-level calculations we identify partons with jets of the same direction in the η,ϕ plane (ϕ being the azimuthal angle). The effects of hadronic energy mismeasurements are included via Gaussian smearing of parton energies and momenta with standard deviation $\sigma=(0.8\ \text{GeV}^{1/2})\sqrt{E_{\text{parton}}}$. A parton is defined as a jet if its transverse momentum and pseudorapidity satisfy the cuts listed in Table II. In addition, we require any electron-jet pair or jet-jet pair to be separated in

$$\Delta R=[(\Delta\phi)^2+(\Delta\eta)^2]^{1/2} \qquad (2)$$

by the minimum values given in Table II.

Figure 1 shows the resulting total cross sections for $W+n$ jets for $n=1,2,3$ vs $\bar{p}p$ c.m. energy $\sqrt{s}$ for three values of the minimum $p_T(W)$ cut: 20, 50, and 100 GeV. Results at multi-TeV pp colliders are essentially identical to those presented here, since the dominant contributions to the cross section involve gluons or sea quarks in the initial state. As the c.m. energy increases, it is expected that a higher jet threshold will be imposed for practical reasons as well as to stay away from the divergence associated with the infrared singularities. While for $W+1$-jet events the effect of increasing the cut can be read off the three curves of Fig. 1(a), some rise with energy of the $p_T(j)$ cut has to be implemented for the multijet events. For simplicity, we have chosen a $p_T(j)$ cut linearly dependent on $\sqrt{s}$:

$$p_T(j) > \left[0.25\left[\frac{\sqrt{s}}{1\ \text{TeV}}\right]+15\right]\ \text{GeV}\ . \qquad (3)$$

This $p_T(j)$ cut corresponds to values of 19 GeV for the LHC (16 TeV), 25 GeV for the SSC (40 TeV), and 40 GeV for the Eloisatron (100-TeV European Long Intersecting Storage Accelerator). The cross sections increase as the c.m. energy grows, due to the fact that the sea-quark and gluon luminosities become larger at higher energies. The slower increases of the cross sections in Figs. 1(b) and 1(c) as compared to Fig. 1(a) are due to the severity of the $p_T(j)$ cut in Eq. (3). The total cross sections of $W(\to e\nu)+n$ jets at the SSC energy for $p_T(W) > 20$ GeV are

TABLE II. Acceptance cuts and energy resolutions used in the calculations for the detector simulation.

	$\sqrt{s}$ (TeV)	0.63	1.8
Charged leptons	$p_T(e)$ (GeV)	15	15
	$\eta(e)$	3.0	2.5
	$\sigma/\sqrt{E}$ ($\text{GeV}^{1/2}$)	0.15	0.15
Jets	$p_T(j)$ (GeV)	10	15
	$\eta(j)$	3.0	2.5
	$\sigma/\sqrt{E}$ ($\text{GeV}^{1/2}$)	0.8	0.8
Separations	ΔR_{ej}	0.7	0.7
	ΔR_{jj}	1.0	0.7
W events	$\not{p}_T$ (GeV)	15	15
	$M_T(e,\not{p}_T)$ (GeV)	50	50
Z events	M_{ee} (GeV)	50	50

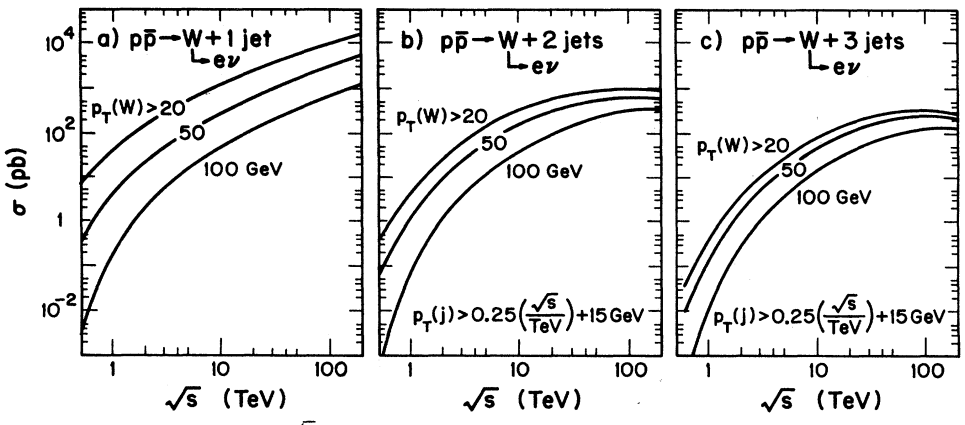

FIG. 1. Total cross sections vs c.m. energy $\sqrt{s}$ for $p\bar{p}\to W+n$ jets with (a) $n=1$, (b) $n=2$, and (c) $n=3$. For events with 2 or 3 jets a transverse-momentum cut was imposed on jets, which becomes more severe at higher-energy colliders.

$$\sigma[W(\to e\nu)+n \text{ jets}]=\begin{cases}4.2 \text{ nb} & \text{for } n=1 \text{ ,}\\ 0.9 \text{ nb} & \text{for } n=2 \text{ ,}\\ 0.3 \text{ nb} & \text{for } n=3 \text{ .}\end{cases}$$

In the calculations of Fig. 1, we have used the parton distribution functions of Eichten, Hinchliffe, Lane, and Quigg[23] (ELHQ) set I, which were particularly developed for calculations at supercolliders. For the later calculations at S$p\bar{p}$S and Tevatron energies, we take the distribution function set I of Duke and Owens.[24] The QCD predictions are based on a $Q^2=\hat{s}$ scale choice; somewhat larger cross sections are obtained with other Q^2 scale choices, as will be discussed in Sec. VI. In the case of 3-jet events, these uncertainties in the absolute normalization can be as large as a factor of 3. Also the matching of the parton-level calculations of multijet production with the experimental jet observations may introduce some further uncertainties, which should be kept in mind in the following.

Figures 2 and 3 show the calculated $W,Z+n$-jet cross sections at these two machines. Parts (a) and (b) give the p_T distributions of the weak boson; parts (c) and (d) show the corresponding cross sections integrated above a minimum p_T cutoff. With 5 pb^{-1} of integrated luminosity, we expect at the S$p\bar{p}$S,

1.5 $W(\to e\nu)+3$-jet events ,

0.2 $Z(\to e\bar{e})+3$-jet events ,

and, at the Tevatron,

21 $W(\to e\nu)+3$-jet events ,

2 $Z(\to e\bar{e})+3$-jet events .

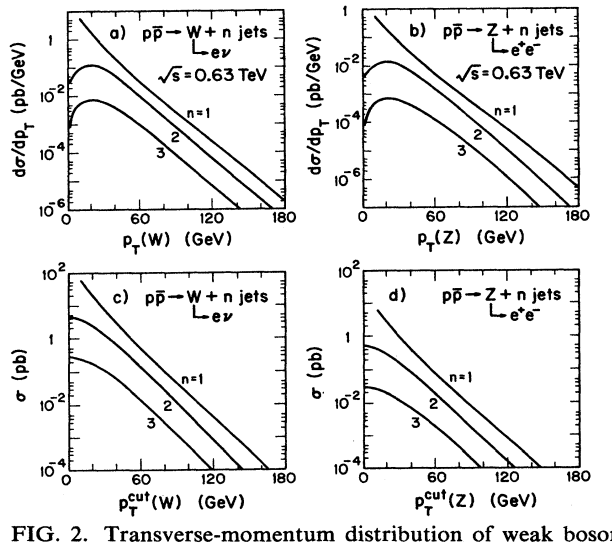

FIG. 2. Transverse-momentum distribution of weak bosons in association with 1, 2, or 3 jets at $\sqrt{s}=0.63$ TeV with cuts as described in Table II, (a) $W(\to e\nu)+n$-jet and (b) $Z(\to e\bar{e})+n$-jet events. The cross sections integrated above a minimum value of (c) $p_T(W)$ and (d) $p_T(Z)$ are shown below the corresponding differential distributions.

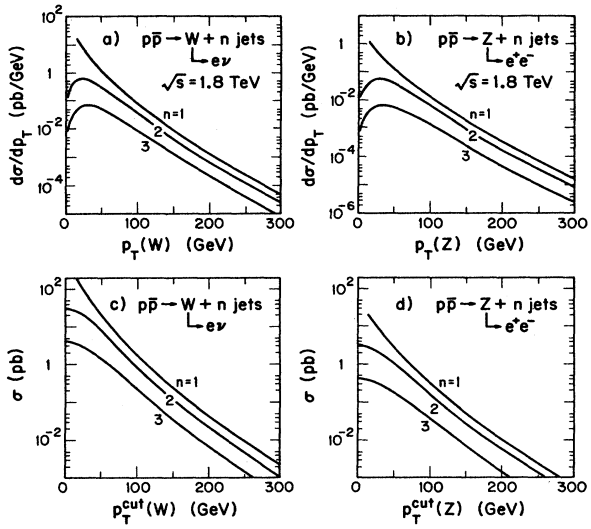

FIG. 3. Same as Fig. 2 but for $\sqrt{s}=1.8$ TeV.

A measure of the relative importance of W or Z events with different numbers of jets is provided by the expected fraction $f^V(n)$ of events with a fixed number n of jets ($n\leq 3$),

$$f^V(n)\equiv\sigma(V+n \text{ jets})\Big/\sum_{i=0}^{3}\sigma(V+i \text{ jets}) \text{ ,} \tag{4}$$

and the fraction $F^V(n)$ of events with $\geq n$ jets,

$$F^V(n)\equiv\sum_{i=n}^{3}\sigma(V+i \text{ jets})\Big/\sum_{i=0}^{3}\sigma(V+i \text{ jets}) \text{ .} \tag{5}$$

Tables III and IV give our estimates of $f^V(n)$ and $F^V(n)$ for $V=W$ and Z. The uncertainty in the entries is due to different choices of the energy scale Q^2 in $\alpha_s(Q^2)$, which we will discuss in the next section.

Similarly, Table V presents the ratio of $W\to e\nu$ to $Z\to e\bar{e}$ events:

$$R_I\left[\frac{W\to e\nu}{Z\to e\bar{e}}\right]\equiv\frac{\sigma(W\to e\nu+n \text{ jets})}{\sigma(Z\to e\bar{e}+n \text{ jets})} \text{ ,} \tag{6}$$

where the subscript I stands for an integrated cross-section ratio. These values are essentially independent of the choice of the Q^2 scale. The ratios defined in Eqs. (4)–(6) are important not only to test the SM, but also to search for new physics. For instance, as shown in Ref. 25, a heavy top quark systematically changes the $W+n$-jet distributions, enhancing the rates at higher n. Other new heavy particles may similarly distort these predictions for $V+$multijet distributions.

Two other distributions which are useful in top-quark searches are shown in Fig. 4, both for the S$p\bar{p}$S and the Tevatron. Figures 4(a) and 4(c) give the $p_T(e)$ distributions and Figs. 4(b) and 4(d) show the $M_T(e,\not{p}_T)$ distributions. Obviously the Jacobian peak in the $p_T(e)$ distribution has been smeared out by the W transverse motion for $n\neq 0$, whereas the corresponding peak in the $M_T(e,\not{p}_T)$ distribution still remains due to the approximate invari-

TABLE III. Predicted fractions of $W(\to e\nu)+n$-jet events, as defined in Eqs. (4) and (5), at S$p\bar{p}$S and Tevatron energies. The uncertainty in the entries is due to the different Q^2 choices. The lower values correspond to $Q^2=\hat{s}$ and the upper values to $Q^2=p_G^2$ for $n>0$ and vice versa for $n=0$.

$\sqrt{s}$ (TeV)	0.63		1.8	
n	$f^W(n)$	$F^W(n)$	$f^W(n)$	$F^W(n)$
0	0.83–0.89	1	0.80–0.86	1
1	0.10–0.14	0.11–0.17	0.12–0.16	0.14–0.20
2	$(0.84–2.6)\times10^{-2}$	$(0.91–2.8)\times10^{-2}$	$(1.7–3.9)\times10^{-2}$	$(2.0–4.5)\times10^{-2}$
3	$(0.5–1.7)\times10^{-3}$	$(0.5–1.7)\times10^{-3}$	$(2.3–6.4)\times10^{-3}$	$(2.3–6.4)\times10^{-3}$

ance of the transverse mass to transverse boosts.[26] As discussed in Ref. 25, a top quark with a mass $m_t<M_W$ would greatly distort the Jacobian peak of the $M_T(e,\not{p}_T)$ distribution of $W\to e\nu$ in association with 2 or 3 jets. Therefore, a detailed comparison of experimental results with these distributions may reveal a top-quark signal or allow an improved lower limit to be placed on its mass.

In e^+e^-+n-jet events the Z peak is the dominant structure of the e^+e^- invariant-mass distribution. The inclusive Drell-Yan (DY) cross sections for $Z,\gamma^*\to e\bar{e}$ production are shown in Figs. 5(a) and 5(b) for the S$p\bar{p}$S and the Tevatron. The solid curves are the results with an order-α_s K factor from QCD corrections

$$K=1+\tfrac{8}{9}\pi\alpha_s(M_{ee}^2) \tag{7}$$

which gives $K\approx1.4$ for $M_{ee}^2\sim M_Z^2$. The dashed curves are for $K=1$. Figures 5(c) and 5(d) are the corresponding cross sections integrated over M_{ee} versus a minimum M_{ee} cutoff. The DY cross sections for $M_{ee}>150$ GeV at the S$p\bar{p}$S and at the Tevatron are about 0.13 and 1.0 pb. With an integrated luminosity of 5 pb^{-1}, there will thus be about 0.7 and 5.0 such events at these colliders. If any excess of DY events over the standard-model prediction is observed, it presumably would indicate the presence of new physics. A heavy Z boson predicted in many extensions of the SM would be one such possibility.

Many new particles such as squarks and gluinos in supersymmetric extensions of the SM or leptoquarks predicted in E_6 models and in composite models[27] could show up as monojet or dijet or multijet events with large $\not{p}_T$. Thus SM $\not{p}_T$ background calculations are needed in the search for such new-physics signals beyond the SM. Within the SM a dominant source of monojet, dijet, or three-jet events balanced by a large $\not{p}_T$ is $Z(\to\nu\bar{\nu})+n$-jet production. In comparison with the $Z\to e\bar{e}$ cross section, one might expect that the corresponding distributions would have similar shapes, with a factor of 6 larger rate for $\nu\bar{\nu}$ corresponding to the ratio of $(Z\to\nu\bar{\nu})/(Z\to e\bar{e})$ branching fractions. After detailed calculations including the detector simulation described above, ratios of 7.7, 8.5, and 9.3 at the Tevatron are found for monojet, dijet, and three-jet events, respectively. The change from the naive value of six is due to the acceptance cuts on charged leptons.

In Figs. 6 and 7 we present the ratios of different leptonic decay channels of the W and Z versus the p_T of the weak boson for production at the S$p\bar{p}$S and at the Tevatron colliders. Parts (a) of these two figures give the ratio

$$R_D\left[\frac{Z\to\nu\bar{\nu}}{Z\to e\bar{e}}\right]\equiv\frac{d\sigma(Z\to\nu\bar{\nu})/dp_T}{d\sigma(Z\to e\bar{e})/dp_T}\ , \tag{8}$$

which is proportional to the ratio of the branching fractions, modulo a correction factor due to the charged-lepton acceptance cuts. The subscript D refers to the ratio of differential cross sections. In Figs. 6(b) and 7(b) we show the W-to-Z ratio

$$R_D\left[\frac{W\to e\nu}{Z\to e\bar{e}}\right]\equiv\frac{d\sigma(W\to e\nu)/dp_T}{d\sigma(Z\to e\bar{e})/dp_T} \tag{9}$$

while Figs. 6(c) and 7(c) give the ratio

$$R_D\left[\frac{Z\to\nu\bar{\nu}}{W\to e\nu}\right]\equiv\frac{d\sigma(Z\to\nu\bar{\nu})/dp_T}{d\sigma(W\to e\nu)/dp_T}\ . \tag{10}$$

Parts (d), (e), and (f) show corresponding ratios R_I [see Eq. (6)] of the distributions integrated over $p_T(V)$ above a minimum $p_T(V)$ cutoff. It was previously suggested[16] that the ratios of $\sigma(\text{monojet})/\sigma(e\bar{e}+1\text{ jet})$ and $\sigma(\text{monojet})/\sigma(e\nu+1\text{ jet})$ could provide an alternative way of counting neutrinos in hadron collisions. By using such ratios for higher jet multiplicity n as well, improved neutrino-counting tests can be performed. The ratios of Eqs. (8) and (9) may suffer from low statistics due to the smallness of the branching fraction of $Z\to e\bar{e}$, though the

TABLE IV. Same as Table III but for $Z(\to e\bar{e})+n$-jet events.

$\sqrt{s}$ (TeV)	0.63		1.8	
n	$f^Z(n)$	$F^Z(n)$	$f^Z(n)$	$F^Z(n)$
0	0.85–0.9	1	0.84–0.89	1
1	0.09–0.13	0.10–0.15	0.09–0.13	0.11–0.16
2	$(0.75–2.3)\times10^{-2}$	$(0.79–2.4)\times10^{-2}$	$(1.4–3.1)\times10^{-2}$	$(1.5–3.6)\times10^{-2}$
3	$(0.42–1.4)\times10^{-3}$	$(0.42–1.4)\times10^{-3}$	$(1.8–5.0)\times10^{-3}$	$(1.8–5.0)\times10^{-3}$

TABLE V. Predicted $W(\rightarrow e\nu)+n$-jet to $Z(\rightarrow e\bar{e})+n$-jet event ratios R_I as defined in Eq. (6) at $S\bar{p}pS$ and Tevatron energies.

$\sqrt{s}$ (TeV)	$n=0$	$n=1$	$n=2$	$n=3$	$n\geq 0$	$n\geq 1$	$n\geq 2$	$n\geq 3$
0.63	7.8	8.6	8.9	9.5	7.9	8.7	8.9	9.5
1.8	7.0	9.1	9.3	9.4	7.3	9.2	9.3	9.4

signal is clean. The small $Z(\rightarrow e\bar{e})+n$-jet counting rate can be avoided by normalizing with respect to the $W(\rightarrow e\nu)+n$-jet rate as in Eq. (10). The two options correspond to a tradeoff between statistical errors and systematic errors. However, as we shall see in the next section, the systematic errors are relatively small due to a cancellation of uncertainties in the ratio, and hence the $(Z\rightarrow\nu\bar{\nu})/(W\rightarrow e\nu)$ ratio of Eq. (10) should be very useful for neutrino counting. In the results presented in Figs. 6 and 7 three generations of light neutrinos are assumed. One additional light $\nu\bar{\nu}$ pair would increase the ratios of parts (a) and (d) in Figs. 6 and 7 by 33%, parts (b) and (e) by 6.7%, and parts (c) and (f) by 25% due to the change in branching fractions. Therefore, precise measurements of these ratios would provide further information on the number of light neutrinos. Note, however, that the ratios of Eqs. (9) and (10) could be also affected by contributions from heavy-top-quark pair production with one t decaying via $t\rightarrow be\nu$, especially for $n\geq 2$ jets.

IV. DISCUSSION OF UNCERTAINTIES

The results presented in the previous section depend somewhat on the assumptions made in our calculations and varying these assumptions will alter our numerical results. These variations are of two kinds: theoretical errors due to our imprecise knowledge of structure functions or the arbitrariness of the choice of scale in the strong coupling constant and "experimental" errors which arise from the need to match experimentally observed quantities, such as the energy deposition inside calorimeters, to parton-level four-momenta, which we used in our simulation. We start by considering these latter uncertainties which can be quantified by varying the kinematical cuts.

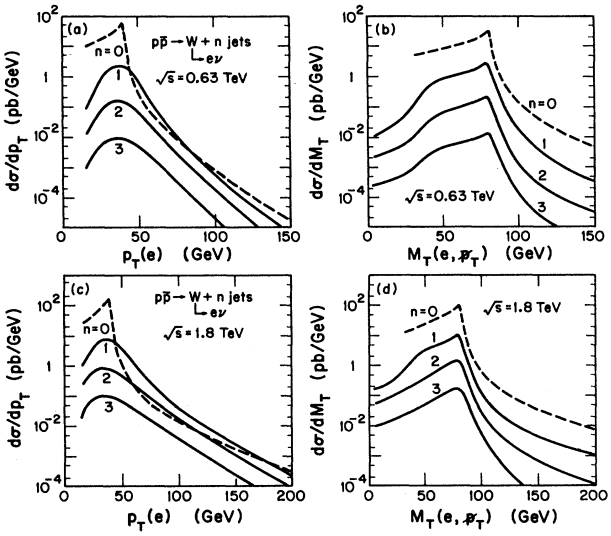

FIG. 4. Distributions of electron transverse momentum $p_T(e)$ and W transverse mass $M_T(e,\not{p}_T)$ for $p\bar{p}\rightarrow W+n$ jets at $\sqrt{s}=0.63$ TeV (a) and (b), and at $\sqrt{s}=1.8$ TeV (c) and (d).

As one might expect the results are not very sensitive to the precise values of the p_T and η cuts on the charged leptons. The insensitivity to the $p_T(e)$ cut is due to the clustering of lepton transverse momenta near the Jacobian peak in the $p_T(e)$ distribution [see Figs. 4(a) and 4(c)]. We also find that small lepton rapidities dominate. Even a very stringent cut such as $|\eta(e)|<1$ reduces the Tevatron $W+3$-jet signal with $|\eta(e)|<2.5$ by 40% only and the $Z+3$-jet signal by 65%. In Figure 8, where we plot the ΔR distributions for $W+2,3$-jet events at the Tevatron, we can see that the leptons are usually well isolated, with minimum electron-jet separations exceeding a median value of $\Delta R\approx 1.5$ even in the $W+3$-jet case.

While the matching of simulated and experimental cuts on the charged leptons should not pose any problem, our predictions depend much more critically on the jet definition. From a theoretical point of view this is obvious, because our tree-level calculations exhibit collinear and infrared singularities which lead to divergent results at small jet-jet separations and at low jet transverse momenta. The collinear singularity shows up in Fig. 8 as a strong enhancement as $\Delta R_{jj}\rightarrow 0$. The effect of this singularity at small ΔR_{jj} is somewhat mitigated by the peak around $\Delta R_{jj}=\pi$, which is of kinematical origin. As a result the cross sections are not very sensitive to the actual value of the jet separation cut. Increasing the cut from $\Delta R_{jj}>0.7$ to $\Delta R_{jj}>1.0$ reduces the $W+3$-jet rate by less than 25% at the Tevatron energy.

By contrast, the dependence on the $p_T(j)$ cutoff is much more dramatic. Figures 9(a) and 9(b) show the $p_T(j)$ distributions for the slowest jet and Figs. 9(c) and 9(d) show the cross sections integrated above a $p_T(j)$ cutoff, for $W+n$-jet events at the Tevatron. Increasing the $p_T(j)$ cut from 10 to 15 to 20 GeV reduces the integrated cross section from 11 to 3.9 to 1.7 pb for $W+3$-jet events at the Tevatron. The correct matching of parton-level transverse momenta with experimentally observed jet values is mainly a problem of detector and hadronization modeling which can be solved by gauging against purely QCD-induced multijet events.

In addition to these experimental uncertainties there are several theoretical ambiguities in the calculations. We have first studied variations arising from the different

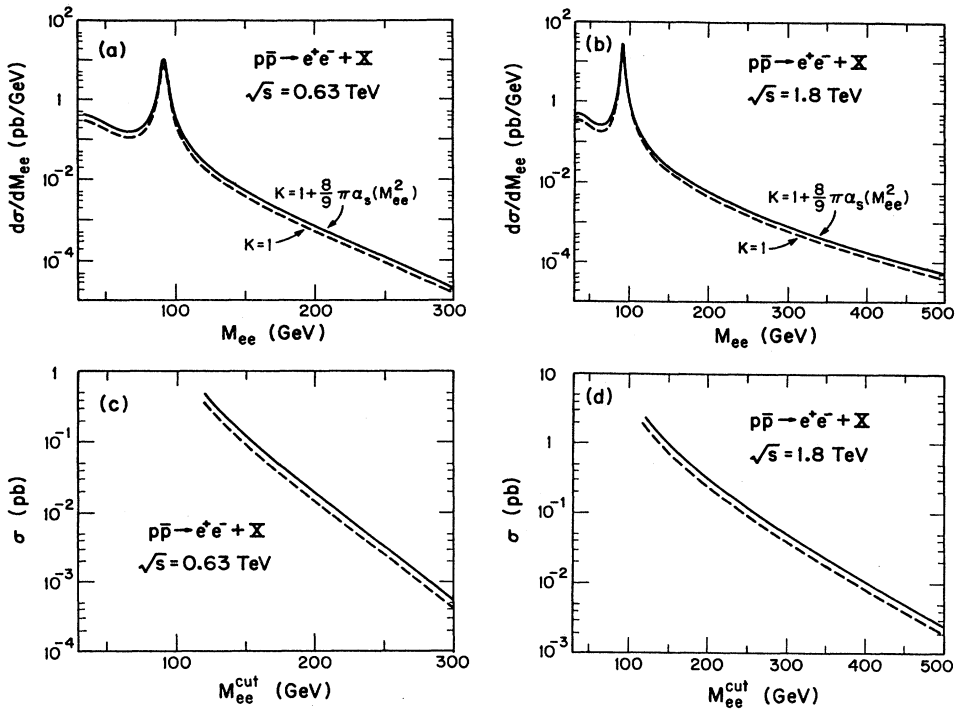

FIG. 5. Invariant-mass distribution for $p\bar{p} \to e^+e^- + X$ at (a) $\sqrt{s} = 0.63$ TeV and (b) $\sqrt{s} = 1.8$ TeV. The cross sections integrated above a minimum value of M_{ee} are shown in (c) and (d) below the corresponding differential distributions. The solid curves correspond to the results with an order-α_s K factor as defined in Eq. (7); the dashed curves are those with $K = 1$.

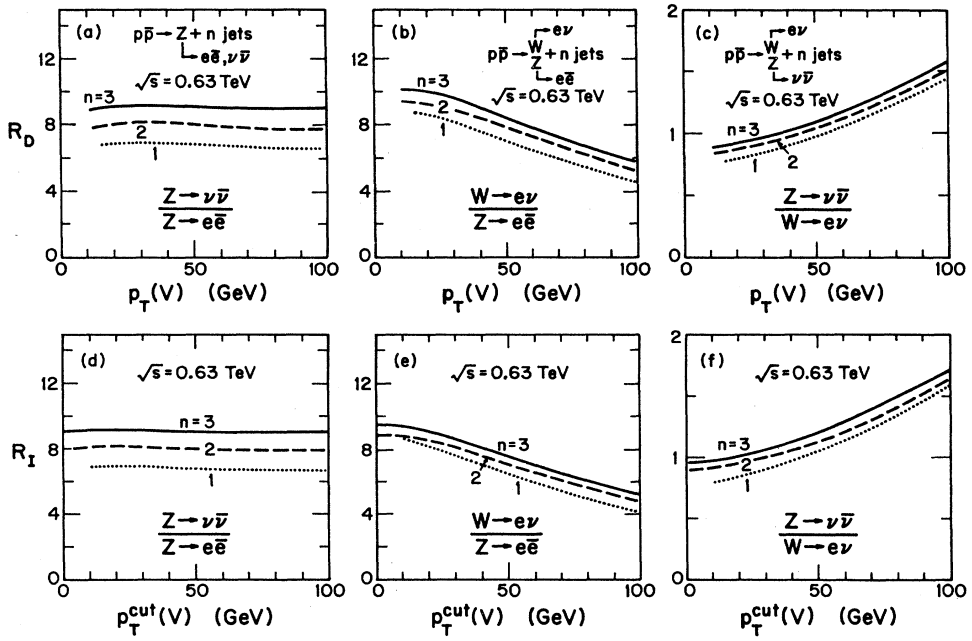

FIG. 6. Ratios of differential $p_T(V)$ distributions (a) $R_D(Z \to \nu\bar{\nu}/Z \to e\bar{e})$, (b) $R_D(W \to e\bar{\nu}/Z \to e\bar{e})$, (c) $R_D(Z \to \nu\bar{\nu}/W \to e\bar{\nu})$, as defined in Eqs. (8)–(10) vs transverse momentum of the weak bosons at $\sqrt{s} = 0.63$ TeV. Ratios (R_I) of the cross sections integrated above a minimum value of $p_T(V)$ are shown below the corresponding differential ratios.

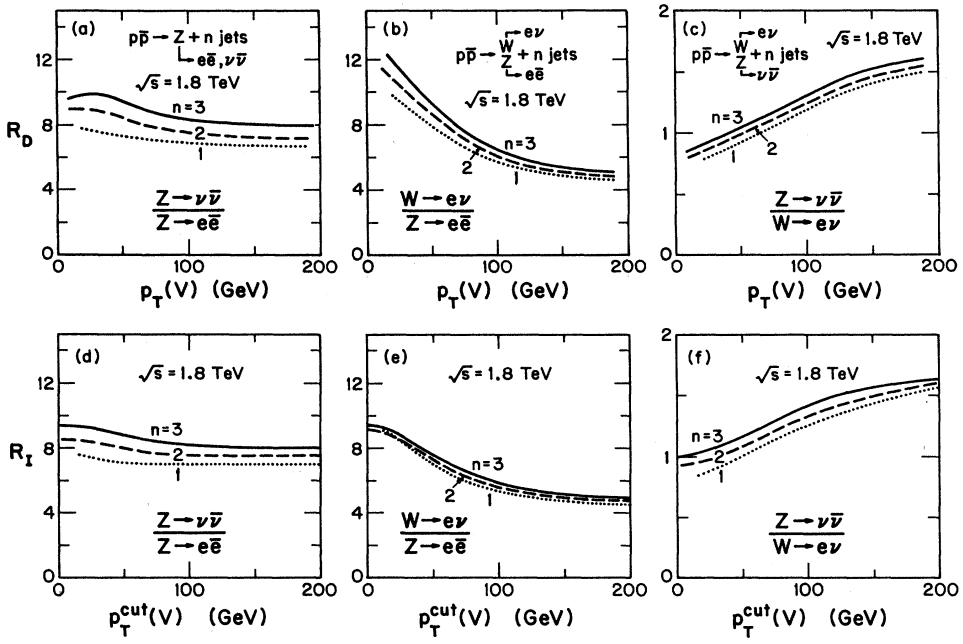

FIG. 7. Same as Fig. 6 but for $\sqrt{s} = 1.8$ TeV.

choices of parton distribution functions and we found that there was no appreciable difference in our results using the structure-function set I of EHLQ (Ref. 23) and set I of Duke and Owens.[24]

A much larger source of uncertainty is the choice of energy scale Q^2 in the strong coupling constant $\alpha_s(Q^2)$. Since the $W,Z+n$-jet cross sections are proportional to $(\alpha_s)^n$ the QCD predictions at the tree level can be changed substantially, especially for $W,Z+3$-jet events. Without one-loop calculations available to reduce this scale uncertainty the proper choice of scale may be regarded as a fit parameter in the comparison of theory and experiment.

In the calculations presented thus far, we have made the choice $Q^2=\hat{s}$, the subprocess c.m. energy squared, in the evaluation of the QCD running coupling constant $\alpha_s(Q^2)$. We have also studied four other choices for Q^2: namely, (i) the W-boson mass squared $Q^2=M_W^2$; (ii) the W transverse energy squared $Q^2=E_T^2(W)=M_W^2+p_T^2(W)$; (iii) the arithmetic average of $p_T(j)$ squared $Q^2=\overline{p_A^2}\equiv(1/n)\sum_i^n p_{Ti}^2$; (iv) and the geometrical average of $p_T(j)$ squared $Q^2=\overline{p_G^2}\equiv(\prod_i^n p_{Ti}^2)^{1/n}$. The ratios of

$$R(Q^2/\hat{s}) \equiv \frac{d\sigma(Q^2)/dp_T}{d\sigma(Q^2=\hat{s})/dp_T} \tag{11}$$

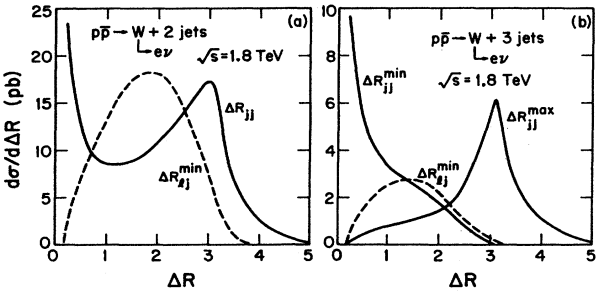

FIG. 8. Minimum and maximum jet-jet separations ΔR_{jj} and minimum lepton-jet separations ΔR_{lj} for (a) $W+2$-jet and (b) $W+3$-jet events at $\sqrt{s}=1.8$ TeV.

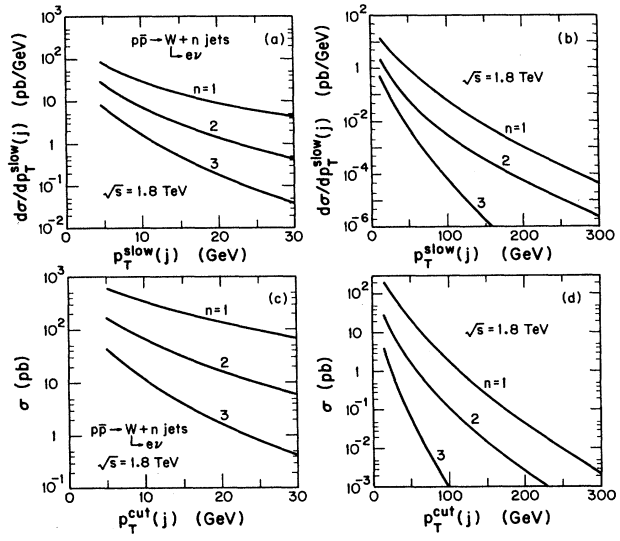

FIG. 9. Transverse-momentum distribution of the slowest jet for $p\bar{p} \to W+n$ jets at the Tevatron. The cross sections integrated above a minimum value of $p_I(j)$ are also shown below the corresponding differential distributions. (a) and (c) are for a lower-$p_T(j)$ region.

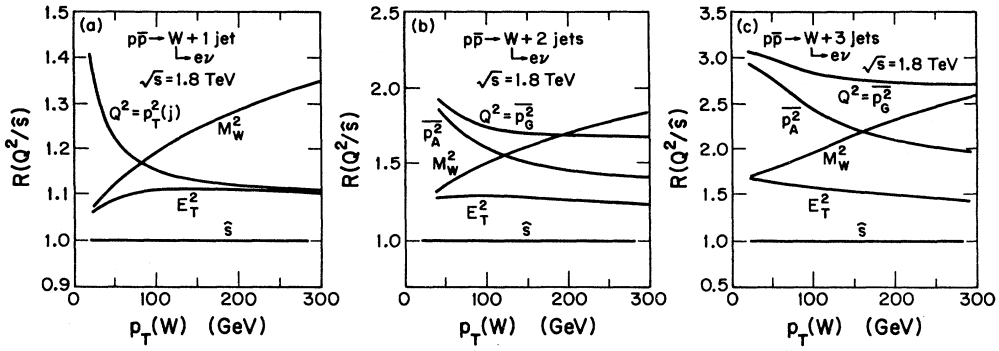

FIG. 10. $p_T(W)$ distributions for different choices of $\alpha_s(Q^2)$ for $p\bar{p}\to W+n$ jets for (a) $n=1$, (b) $n=2$, and (c) $n=3$ at the Tevatron. The choices of Q^2 are described in the text. The curves are normalized with respect to the distribution with $Q^2=\hat{s}$, defined as $R(Q^2/\hat{s})$ in Eq. (11).

for $W+n$-jet processes at the Tevatron are shown in Fig. 10 for $n=1,2,3$. The choice of $Q^2=\hat{s}$ gives the smallest production of monojet, dijet, or 3-jet events balanced by a large $\not{p}_T$ and an electron.

As is apparent from Fig. 10 the actual 3-jet rates may be larger by up to a factor of 3 than the results with the $Q^2=\hat{s}$ scale choice. This large theoretical uncertainty which is introduced by the arbitrariness of the scale choice at the tree level immediately poses the question to what extent the ratios of cross sections presented in Sec. III are uncertain as well. In the $(Z\to\nu\bar{\nu})/(W\to e\nu)$ ratios, for example, a factor of 3 error would render completely unobservable the effect of a fourth neutrino species, which would enhance this ratio by 25%. We find, however, that varying the scale Q^2 has practically identical effects on the $W+n$-jet and $Z+n$-jet spectra. The ratios of the $p_T(Z)$ distributions to the analogous $p_T(W)$ distributions in Fig. 10 never differ by more than 3% for the various Q^2-scale choices. Hence the ratios of W/Z distributions and the $(Z\to\nu\bar{\nu})/(Z\to e\bar{e})$ ratios are completely unaffected by changing the scale Q^2, and similarly we expect other uncertainties to cancel in the same manner. The ratios presented in Sec. III should thus be reliable at the few percent level in the low-$p_T(V)$ region, which corresponds to the numerical uncertainty of our Monte Carlo simulations. Even in the high-p_T region this numerical error does not exceed 10%.

V. CONCLUSIONS

In this paper we have systematically studied $V+n$-jet production ($n\leq 3$) in high-energy $p\bar{p}$ collisions for $V=W$, Z, or γ^*. Our calculations are based on complete tree-level evaluations of $V+(n+2)$-parton amplitudes in the framework of perturbative QCD, using amplitude techniques. We have checked our numerical tools against other independent calculations and found excellent agreement.

The resulting distributions of $p_T(V)$, $p_T(e)$, $M_T(e,\not{p}_T)$, and M_{ee} in V production in association with n jets are important for studying the properties of V production and for understanding backgrounds in new-physics searches. We have presented predictions for the $(Z\to\nu\bar{\nu})/(Z\to e\bar{e})$ and $(Z\to\nu\bar{\nu})/(W\to e\nu)$ ratios which may be used in neutrino counting. These ratios are essentially independent of the choice of scale in the strong coupling constant.

Our results are in general not very sensitive to the lepton acceptance cuts; however, n-jet production rates are very sensitive to the jet definition, in particular to the $p_T(j)$ cutoff. The uncertainty from the parton distribution functions is not appreciable. The main theoretical uncertainty rather arises from the arbitrariness, at the tree level, of the QCD energy evolution scale Q^2, which enters the running coupling constant $\alpha_s(Q^2)$. The scale choice of $Q^2=\hat{s}$ gives the most conservative production rates, while other possible choices lead to predictions of the cross sections which are larger by as much as a factor of 2–3. The ratios of cross sections presented in Sec. III are essentially free of these uncertainties, however, and should provide for excellent tests of the standard model.

ACKNOWLEDGMENTS

We thank W. J. Stirling and W. Giele for their help and cooperation in comparing their and our computer codes. This research was supported in part by the University of Wisconsin Research Committee with funds granted by the Wisconsin Alumni Research Foundation, and in part by the U.S. Department of Energy under Contract No. DE-AC02-76ER00881.

[1]UA1 Collaboration, G. Arnison *et al.*, Phys. Lett. **122B**, 103 (1983); **126B**, 398 (1983); **134B**, 469 (1984); **147B**, 241 (1984); UA2 Collaboration, M. Banner *et al.*, *ibid.* **122B**, 476 (1983); UA2 Collaboration, P. Bagnaia *et al.*, *ibid.* **129B**, 130 (1983); Z. Phys. C **24**, 1 (1984).

[2]UA1 Collaboration, D. Denegri, in *Proton-Antiproton Collider Physics,* proceedings of the 6th International Conference, Aachen, West Germany, 1986, edited by K. Eggert, H. Faiss-

ner, and E. Radermacher (World Scientific, Singapore, 1987); UA2 Collaboration, S. Loucatos, *ibid.*

[3]CDF Collaboration, F. Abe *et al.*, Phys. Rev. Lett. **62**, 1005 (1989).

[4]G. Altarelli *et al.*, Nucl. Phys. **B246**, 12 (1984); Z. Phys. C **27**, 617 (1985); P. Arnold and M. H. Reno, Nucl. Phys. **B319**, 37 (1989); P. Arnold, R. K. Ellis, and M. H. Reno, Phys. Rev. D **40**, 912 (1989).

[5]S. D. Ellis, R. Kleiss, and W. J. Stirling, Phys. Lett. **154B**, 435 (1985); R. Kleiss and W. J. Stirling, Nucl. Phys. **B262**, 235 (1985); Phys. Lett. B **180**, 171 (1986).

[6]J. F. Gunion, Z. Kunszt, and M. Soldate, Phys. Lett. **163B**, 389 (1985); **168B**, 427(E) (1986); J. F. Gunion and M. Soldate, Phys. Rev. D **34**, 826 (1986).

[7]R. K. Ellis and R. J. Gonsalves, in *Supercollider Physics,* proceedings of the Topical Conference, Eugene, Oregon, 1985, edited by D. E. Soper (World Scientific, Singapore, 1986).

[8]V. Barger, T. Han, J. Ohnemus, and D. Zeppenfeld, Phys. Rev. Lett. **62**, 1971 (1989).

[9]F. A. Berends, W. T. Giele, H. Kuijf, R. Kleiss, and W. J. Stirling, Phys. Lett. B **224**, 237 (1989).

[10]K. Hagiwara and D. Zeppenfeld, Nucl. Phys. **B313**, 560 (1989).

[11]F. A. Berends, W. T. Giele, and H. Kuijf, Nucl. Phys. **B321**, 39 (1989).

[12]H. Baer, V. Barger, H. Goldberg, and J. Ohnemus, Phys. Rev. D **38**, 3467 (1988); S. Dawson and S. Godfrey, *ibid.* **39**, 221 (1989).

[13]R. N. Cahn *et al.*, in *Experiments, Detectors, and Experimental Areas for the Supercollider,* proceedings of the Workshop, Berkeley, California, 1987, edited by R. Donaldson and M. G. D. Gilchriese (World Scientific, Singapore, 1988), p. 20; J. F. Gunion *et al.*, *ibid.*, p. 110; V. Barger, in *Proceedings of the XXIV International Conference on High Energy Physics,* Munich, West Germany, 1988, edited by R. Kotthaus and J. H. Kühn (Springer, Berlin, 1988), p. 1265.

[14]H. Baer *et al.*, Phys. Rev. D **36**, 96 (1987); J. F. Gunion *et al.*, Int. J. Mod. Phys. A **2**, 1145 (1987).

[15]For a review and references to E_6 models, see J. L. Hewett and T. G. Rizzo, Phys. Rep. (to be published).

[16]F. Halzen and K.-I. Hikasa, Phys. Lett. **168B**, 135 (1986), and references therein.

[17]For recent analyses see, e.g., H. Baer, V. Barger, and R. J. N. Phillips, Phys. Rev. D **39**, 3310 (1989); J. Rosner, *ibid.* **39**, 3297 (1989); P. Agrawal and S. D. Ellis, Phys. Lett. B **221**, 393 (1989).

[18]K. Hagiwara and D. Zeppenfeld, Nucl. Phys. **B274**, 1 (1986).

[19]D. Zeppenfeld, W. Long, and T. Han (in preparation). The programs, written in standard FORTRAN-77, are available upon request.

[20]F. A. Berends and W. T. Giele, Nucl. Phys. **B294**, 700 (1987), and references therein.

[21]F. A. Berends and W. T. Giele, Nucl. Phys. **B306**, 759 (1988).

[22]N. K. Falck, D. Graudenz, and G. Kramer, Phys. Lett. B **220**, 299 (1989).

[23]E. Eichten, I. Hinchliffe, K. Lane, and C. Quigg, Rev. Mod. Phys. **56**, 579 (1984).

[24]D. W. Duke and J. F. Owens, Phys. Rev. D **30**, 49 (1984).

[25]H. Baer, V. Barger, and R. J. N. Phillips, Phys. Lett. B **221**, 398 (1989).

[26]V. Barger, A. D. Martin, and R. J. N. Phillips, Z. Phys. C **21**, 99 (1983).

[27]V. Barger, K. Hagiwara, T. Han, and D. Zeppenfeld, Phys. Lett. B **220**, 464 (1989).